Spectroscopic properties of $SrRE_2O_4$: Eu^{3+} (RE identical to Eu, Gd, Y and In): crystal-field analysis and paramagnetic susceptibility measurements

1993 J. Phys.: Condens. Matter 5 5201

(http://iopscience.iop.org/0953-8984/5/29/015)

J. Phys.: Condens. Matter 5 (1993) 5201–5208. Printed in the UK

Spectroscopic properties of $SrRE_2O_4$: Eu^{3+} (RE ≡ Eu, Gd, Y and In): crystal-field analysis and paramagnetic susceptibility measurements

M'hamed Taibi†‡, Elizabeth Antic-Fidancev†, Jilali Aride‡, Michèle Lemaitre-Blaise† and Pierre Porcher†

† Laboratoire des Eléments de Transition dans les Solides, UPR 210 du CNRS, 1 Place A Briand, F-92195 Meudon, France

‡ Laboratoire de Physico-Chimie des Matériaux, Ecole Nationale Supérieure de Takaddoum, BP 5118 Rabat, Morocco

Received 16 January 1993, in final form 10 May 1993

Abstract. The luminescence properties of trivalent europium embedded in an isostructural $SrRE_2O_4$ (RE ≡ Eu, Gd, Y, In) series have been studied. The energy level schemes as well as the crystal-field analysis of the two non-equivalent point sites present in the structure show clearly the smooth modifications of the europium local probe environment for only one point site versus the ionic radius of the cation, the environment of the other site being quite unmodified. The paramagnetic susceptibility of the europium compound is well reproduced by using the wavefunctions derived from the crystal-field calculation.

1. Introduction

In previous articles we studied the optical properties of some of the stoichiometries found in the RE_2O_3–BaO–ZnO chemical system [1,2]. This system is related to the RE_2O_3–BaO–CuO system but is transparent from IR to UV wavelength ranges. We focused our attention on RE_2BaZnO_5, isostructural to RE_2BaCuO_5, which is found as an impurity phase in superconducting materials [3]. Moreover, it is interesting to replace the barium ion by other alkaline earths such as Sr and Ca. In this way it occurred to us that it would be interesting to study the optical properties of the alkaline-earth–rare-earth oxides (plus indium) MRE_2O_4, considered as precursor materials for synthesis of the ternary oxides. These compounds have been known for years [4–8] but the purpose of the present study is to obtain a better comprehension of their optical properties. To achieve this, the classical Eu^{3+} [9–11] spectroscopic probe has been introduced into the matrices. Another goal of the work is to emphasize the structure–optical properties relation, and in particular to see how the limit of existence of these phases is translated in terms of rare-earth optical properties.

2. Experiment

2.1. Sample preparation

$SrEu_2O_4$ and $SrRE_2O_4$:2% Eu^{3+} (RE ≡ Gd, Y, In) were prepared using high-purity starting oxides. The stoichiometric mixture of the intimately ground rare-earth oxides and strontium

0953-8984/93/295201+08$07.50

carbonate is fired at 900 °C for 24 h and then at 1400 °C for 48 h. The resulting compounds, checked by the x-ray technique, appeared to be of a single phase. Good crystallinity of the samples was observed from the emission linewidth [9], as well as from the x-ray technique.

2.2. Optical measurements

The optical absorption spectrum was measured only for $SrEu_2O_4$ at room temperature and liquid-nitrogen temperature with a commercial Cary 2400 spectrometer. The site-unresolved fluorescence excitation was made using the 457.9 nm line of a 5W CW argon ion laser, whereas the site-selective excitation is made through a rhodamine 6G dye laser excitation on the respective $^5D_0 \rightarrow {}^7F_0$ transition of the chosen crystallographic site. The fluorescence emission was recorded by standard techniques at 10, 77 and 300 K.

2.3. Magnetic measurements

The paramagnetic susceptibility of pure $SrEu_2O_4$ was measured using a DMS5 suspended magnetometer between 2 and 300 K. All measurements included diamagnetic correction of the elements. The paramagnetic susceptibility was found to be independent of the magnetic field in the temperature range of our measurements.

2.4. Crystal structure

In their review of the MO–RE_2O_33 (M ≡ Ca, Sr, Ba; RE ≡ Gd, Ho, Yb, Y) binary system, Barry and Roy [12] classified the compounds into three classes, roughly corresponding to three alkaline-earth cations:

(1) CaY_2O_4 and $CaHo_2O_4$;
(2) $CaYb_2O_4$, $SrGd_2O_4$, SrY_2O_4, $SrHo_2O_4$ and $SrYb_2O_4$;
(3) $BaGd_2O_4$, BaY_2O_4, $BaHo_2O_4$ and $BaYb_2O_4$.

For the series that we are at present interested in, Muller-Buschbaum [13] established the crystal structure of SrY_2O_4, and Pepin [14] extended the determination of the cell parameters to RE ≡ Sm–Lu, In and Y. These compounds are isostructural to $CaFe_2O_4$ and belong to the orthorhombic system (space group, Pnma D_{2h}^{16}, No. 62). In that structure the RE element is located at two 4c positions corresponding to a C_s point site symmetry. For both sites, RE is sixfold coordinated. It clearly appears (figure 1) that one site (site II) is more regular; its point symmetry is relatively close to C_{2v}. This site has the larger volume and longer average bonding distances. Thus, we can suppose that it is less sensitive to a variation in the ionic radius of the cation RE. In this way we can relate the 'optical' and the 'crystallographic' sites.

2.5. Theoretical treatment of energy level scheme

The $4f^6$ configuration of the Eu^{3+} ion is one of the largest of the ground-state configurations of the rare-earth elements, involving 3003 (αSLJM) determinantal states. The energy level scheme is spread over about 200 000 cm^{-1}. The nearest excited configuration $4f^55d$ partially overlaps the ground-state configuration with the lowest states situated at about 70 000 cm^{-1}. In practice the energy level scheme derived from absorption, emission and/or excitation spectroscopy yields only a few terms of the 119 possible terms of the $4f^6$ configuration. For example, in the case of Eu^{3+} embedded in rare-earths oxyhalides, only ^7F, ^5D, ^5L (in part) and ^5G (in part) are observed [10, 11]. Naturally, these reduced data are not sufficient for determining the configuration. The relatively large number of free-ion parameters (the

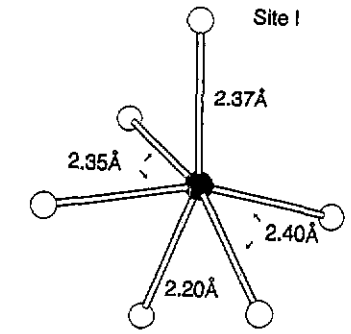

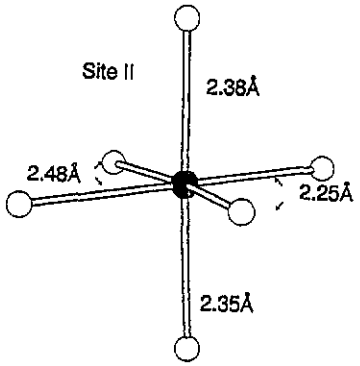

Figure 1. Local symmetries of the RE^{3+} cation in SrY_2O_4. Note that the bonding distances are slightly different from those indicated in [13].

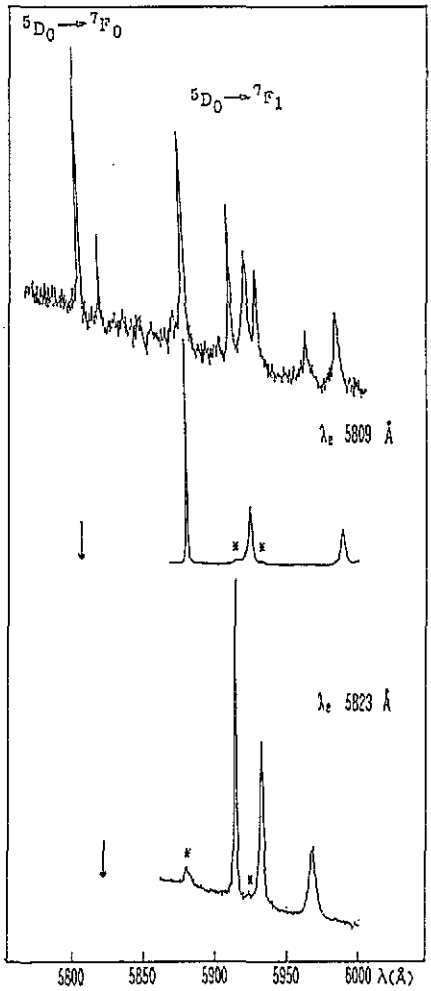

Figure 2. Part of the emission spectrum of SrY_2O_4: Eu^{3+} at 77 K.

Racah and two- and three-body interactions) introduced by the classical theories cannot be considered as adjustable in the experiment and are thus fixed to the extrapolated values [15]. On the contrary a large number of transitions between Stark levels permits good determination of the crystal field (CF) parameters. The one-electron CF Hamiltonian H_{CF} consists of a sum of products of the B_q^k-parameters and the spherical tensors C_q^k appropriate to the site symmetry of the Eu^{3+} ion:

$$H_{CF} = \sum_{k=0}^{6} \sum_{q \geqslant -k}^{q \leqslant k} \left[B_q^k \left(C_q^k + (-1)^q C_{-q}^k \right) + \mathrm{i} S_q^k \left(C_q^k - (-1)^q C_{-q}^k \right) \right].$$

For the C_s point symmetry all B_q^k and S_q^k with k and q even are invariant under all symmetry operations, giving 15 parameters, whereas all S_q^k vanish for C_{2v}, reducing the number of parameters to nine. The secular determinant can be divided into two submatrices of about

1500 × 1500, according to the two values of the crystalline quantum number μ. However, the ^7F ground-state term is well isolated from the rest of the configuration and it alone has that multiplicity. This is why the CF parameters can be determined accurately on a very reduced 49 × 49 submatrix corresponding to the ^7F ground-state term [16]. On such a reduced basis, only the CF operator is involved if the ^7F_J barycentres are adjusted to their experimental values. All computations are performed on a PC by the routines REEL and IMAGE [16]. The standard least-squares method was carried out in order to optimize the B_q^k-parameters. The RMS deviation σ between experimental and calculated energy levels as well as the residue $\sum(E_{exp} - E_{calc})^2$ were used as figures of merit for the quality of the fit.

2.6. Theoretical treatment of the paramagnetic susceptibility

The effect of an externally applied magnetic field on an energy level i is reproduced by the Van Vleck formula, which is derived from the perturbation theory [17]:

$$\chi_i = N\beta^2\left[\frac{\langle\phi_i^{(0)}|\hat{\sigma}|\phi_i^{(0)}\rangle^2}{kT} - 2\sum_{j\neq i}\frac{\langle\phi_i^{(0)}|\hat{\sigma}|\phi_j^{(0)}\rangle\langle\phi_j^{(0)}|\hat{\sigma}|\phi_i^{(0)}\rangle}{E_i - E_j}\right].$$

In this formula, N is the Avogadro number, β is the Bohr magneton, and E_i and E_j are the non-perturbed energy levels. $\hat{\sigma}$ is the magnetic dipole operator $L + g_eS$ represented by a first-rank tensor having three components which characterize the magnetic anisotropy. The expression of the non-perturbed wavefunctions ϕ is obtained from the diagonalized of the secular determinant of the entire configuration. However, the symmetry is restricted here to the C_{2v} symmetry, as a consequence of RAM limitations in the PC and in order to save computing time. The total macroscopic paramagnetic susceptibility and its temperature dependence are derived from the above formula by summing over the thermally populated energy levels, according to Boltzmann statistics.

3. Results and discussion

3.1. Analysis of the data

The fluorescence emission of the $SrRE_2O_4$ compounds is relatively intense, whatever the cation RE. When excited by the 457.9 nm line of the CW argon ion laser, the fluorescence emissions from the $^5D_2$ and $^5D_1$ are observed for all matrices, except at room temperature for which the emissions are quenched. On the contrary the $^5D_0$ level emits intensively, except for the pure europium compound. The presence of two lines for $^5D_0 \rightarrow {}^7F_0$ transition (figure 2) indicates two point sites of low symmetry (C_s, C_n or C_{nv}) for the rare earth, as a consequence of the application of the group theory selection rules for electric dipole transitions [18]. Almost all $^5D_0 \rightarrow {}^7F_J$ transitions are observed without selection rules. This feature indicates a point symmetry not higher than C_{2v}, which is in agreement with the crystallographic data. A dye laser excitation on each $^5D_0 \rightarrow {}^7F_0$ transition permits site-selective excitation of the fluorescence with a very reduced energy transfer between the two sites. For each site, almost all possible transitions are observed, which confirms the C_s point symmetry. The corresponding energy schemes were constructed for the $^7F_1$, $^7F_2$, $^7F_3$ and $^7F_4$ levels (table 1), which constitutes a basis large enough for accurate CF calculations.

The experimental data derived from the fluorescence measurements also constitute an excellent means of testing the nature of the chemical bond when a series of isostructural matrices is involved. Figure 3(*a*) shows the variation in the $^7F_1$ splitting for two sites of the

Table 1. Experimental energy level schemes of Eu^{3+} in $SrRE_2O_4$ at 77 K.

	Energy (cm^{-1})					
	$SrGd_2O_4$		SrY_2O_4		$SrIn_2O_4$	
Level	Site I	Site II	Site I	Site II	Site I	Site II
$^7F_0$	0	0	0	0	0	0
$^7F_1$	208	276	212	273	248	273
	339	321	340	324	341	329
	554	414	520	421	463	417
$^7F_2$	811	809	800	806	788	793
	—	831	917	828	873	—
	1007	984	993	978	985	986
	1190	1113	1170	1118	1140	—
	1257	1162	1251	1165	1202	—
$^7F_3$	1846	1925	1835	1926	1808	1913
	1873	1944	1869	1951	1865	1962
	1911	2008	1902	2008	1900	—
	2013	2038	1998	2054	—	2054
	2037	—	2034	—	2007	—
	2096	—	2086	—	2059	—
	2135	—	2127	—	—	—
$^7F_4$	2667	—	2654	2657	2596	2659
	2768	2685	2759	2690	2740	2711
	2811	—	2802	2796	2768	—
	3063	3032	3052	3052	3028	3023
	3095	3139	3085	3144	3086	—
	3121	3156	3117	3166	3113	3162
	3126	3207	3132	3221	3140	3217
	—	—	3186	—	3167	3260
	3210	—	3210	—	3197	—
$^5D_0$	17232	17176	17214	17176	17187	17175

series. It is clear that the $^7F_1$ splitting of site II (as well as the splitting of other ^7F_J levels) does not vary versus the ionic radius of the cation RE. This is why the CF calculations will be performed in only one case for such a site. For site I, on the contrary, the $^7F_1$ splitting decreases smoothly with decrease in the RE ionic radius (figure 3(*b*)). When plotted on the same abcissa scale, the variation in the $^5D_0 \rightarrow {}^7F_0$ position (figure 3(*c*)) confirms the difference between the two sites; the $^5D_0 \rightarrow {}^7F_0$ position does not vary for site II, whereas its position is lowered when the ionic radius of the cation decreases in site I. Such features suggest study of the scandium compounds for which a crossover of the $^5D_0 \rightarrow {}^7F_0$ positions could be expected. In fact, we were not able to synthesize this compound, or even In–Sc or Y–Sc solid solutions rich in Sc. The analysis of the spectroscopic properties helps to determine the limits of existence of the SrO–RE_2O_3 chemical system. If the RE ionic radius was about 0.76 Å, the two sites should be equivalent.

3.2. Crystal-field simulation

Simulation of the energy level scheme is made for the two sites. Two point symmetries are tested: C_{2v} and C_s. The simulations in the C_{2v} group involving nine parameters were relatively simple to perform, yielding a low σ and residue. The CF parameter set deduced constitutes a good set of starting values for refinement in the C_s symmetry involving 15

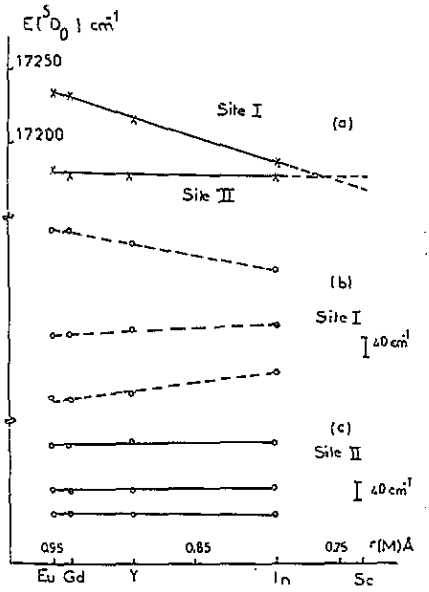

Figure 3. Variation of energy levels versus the ionic radius of the cation RE^{3+}. (*a*) The $^5D_0$ position of the two point sites. (*b*) The $^7F_1$ position for the site I. (*c*) The $^7F_1$ position for the site II.

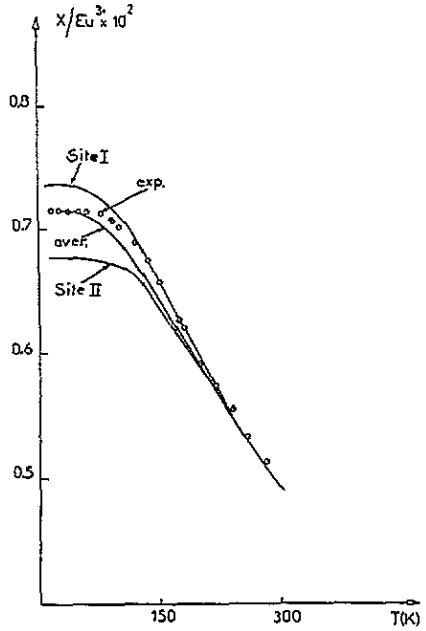

Figure 4. Experimental and calculated paramagnetic susceptibility.

parameters. The number of CF parameters is immediately reduced to 14 by appropriate rotation around the main axis of the reference axis system, which cancels the S_2^2-parameter.

When no polarization measurements are available, i.e. no knowledge of the irreducible representation associated with the CF levels, the simulation procedure proceeds as follows. The first step is to consider the $^7F_1$ level involving only the CF parameters B_q^2. Three sets of these parameters are then deduced and fixed. The second step considers $^7F_1 + {}^7F_2$ together, involving B_q^2 and B_q^4. Three simulations are attempted owing to the three sets of B_q^2, and only one set is finally satisfactory. The remaining B_q^6-parameters are deduced when $^7F_3 + {}^7F_4$ are introduced into the simulation.

For site I, the simulations are performed for the three matrices (table 2) whereas only one simulation is attempted for site II (table 3) on SrY_2O_4 Eu^{3+} as a consequence of non-variation in the energy level positions. Although the number of CF parameters increases, the simulation in C_s symmetry constitutes a real improvement with a better RMS σ and a very small residue. For both simulations the real parts of the CF parameters vary smoothly with the cation, whereas the tendency is not very clear for the imaginary part. This last feature—which is usual in this type of simulation—is probably a consequence of the algorithm used in the standard routines for diagonalization of complex matrices.

3.3. Paramagnetic susceptibility calculation

The experimental results are presented in figure 4. At temperatures lower than 30 K a rapid increase in χ when the temperature decreases is observed. It is due to a small amount of highly paramagnetic impurities, necessarily Eu^{2+}. The estimated concentration which is easily calculated from the large value of the Eu^{2+} effective magnetic moment (11.2 μ_B) is

Table 2. Crystal-field parameters of Eu^{3+} (site I) in $SrRE_2O_4$.

	Value (cm^{-1})					
	$SrGd_2O_4$		SrY_2O_4		$SrIn_2O_4$	
Parameter	C_{2v}	C_s	C_{2v}	C_s	C_{2v}	C_s
B_0^2	78	66	115	129	76	85
B_2^2	609	613	579	580	443	439
B_0^4	− 457	− 483	− 326	− 304	− 263	− 281
B_2^4	−1997	−1994	−2079	−2063	−2088	−2101
S_2^4	—	162	—	63	—	137
B_4^4	1064	1026	1114	1075	1272	1254
S_4^4	—	− 100	—	142	—	26
B_0^6	− 629	− 573	− 760	− 640	− 863	− 828
B_2^6	230	223	262	222	224	193
S_2^6	—	267	—	255	—	142
B_4^6	581	574	621	684	927	889
S_4^6	—	69	—	317	—	90
B_6^6	556	540	517	531	549	544
S_6^6	—	142	—	409	—	− 188
Levels	23	23	25	25	23	23
RMS	7.5	6.4	8.6	5.6	7.8	4.5
Residual	782	575	1187	340	853	284

Table 3. Crystal-field parameters of Eu^{3+} (site II) in SrY_2O_4.

	Value (cm^{-1})	
	SrY_2O_4	
Parameter	C_{2v}	C_s
B_0^2	14	30
B_2^2	265	266
B_0^4	144	105
B_2^4	−1931	−1937
S_2^4	—	261
B_4^4	1153	1107
S_4^4	—	11
B_0^6	− 161	− 94
B_2^6	575	566
S_2^6	—	66
B_4^6	1121	1111
S_4^6	—	− 70
B_6^6	949	993
S_6^6	—	− 10
Levels	20	20
RMS	8.3	7.2
Residual	749	564

much lower than 0.1%. The impurity concentration is too small to allow its characterization by absorption. The curve presented shows experimental values corrected for the impurity contribution (figure 4).

As the paramagnetic susceptibility is a macroscopic property it is calculated by summing the elementary contribution of each site. As mentioned before, diagonalization on the complete secular determinant is required. The free-ion parameters are fixed to standard values: $E_1 = 5510.0\ cm^{-1}$, $E_2 = 24.22\ cm^{-1}$, $E_3 = 582.0\ cm^{-1}$, $\alpha = 20.0\ cm^{-1}$, $\beta = -640.0\ cm^{-1}$, $\gamma = 1750.0\ cm^{-1}$ [19]. The spin–orbit coupling constant ζ characterizes the position of the ^7F_J barycentres. It differs for each site: $1275.0\ cm^{-1}$ for site I and $1250.0\ cm^{-1}$ for site II. The agreement between experiment and calculation is good (in particular the length and the position of the plateau) but not perfect (figure 4). In fact we have to keep in mind that Eu^{3+} constitutes a special case with a non-magnetic $^7F_0$ ground-state level. At low temperatures when only $^7F_0$ is populated, χ is expressed by the off-diagonal term in the Van Vleck formula, which is a temperature non-dependent second-order term in the perturbation theory. This term is very dependent on the wavefunctions, and the C_{2v} approximation is sufficient to explain the small discrepancy.

References

[1] Taibi M, Aride J, Antic-Fidancev E, Lemaitre-Blaise M, Porcher P and Caro P 1988 *J. Solid State Chem* **74** 329

[2] Taibi M, Aride J, Antic-Fidancev E, Lemaitre-Blaise M and Porcher P 1989 *Phys. Status Solidi* A **115** 523

[3] Bailleul S, Porcher P, Taibi M and Aride J 1991 *C.R. Acad. Sci., Paris, Ser. II* **313** 767

[4] Brixner L H 1967 *J. Electrochem. Soc.* **114** 253

[5] Blasse G and Bril A 1967 *J. Chem. Phys.* **47** 5139

[6] Blasse G and Bril A 1969 *J. Inorg. Nucl. Chem.* **31** 1521

[7] Blanchard M, Linares C and Gaume-Mahn F 1971 *C.R. Acad. Sci., Paris* **272** 1075

[8] Rozdin I A, Plotkin S S, Sharipov Kh T, Porotnikov N V, Pravnichenko S P and Petrov K I 1976 *Izv. Akad. Nauk. SSSR Neorg. Mater.* **12** 1255

[9] Antic-Fidancev E, Lemaitre-Blaise M, Porcher P, Bueno I, Parada C and Saez-Puche R 1991 *Inorg. Chim. Acta* **182** 5

[10] Holsa J and Porcher P 1981 *J. Chem. Phys.* **75** 2108

[11] Holsa J and Porcher P 1982 *J. Chem. Phys.* **76** 2798

[12] Barry T L and Roy R 1967 *J. Inorg. Nucl. Chem.* **29** 1243

[13] Muller-Buschbaum Hk 1968 *Z. Anorg. (Allg.) Chem.* **358** 138

[14] Pepin J 1980 *J. Appl. Crystallogr.* **14** 70

[15] Carnall W T, Goodmann G L, Rajnak K and Rana R S 1989 *J. Chem. Phys.* **90** 3443

[16] Porcher P 1989 Computer routines REEL and IMAGE for the simulation of d^N and f^N configurations involving the real and imaginary crystal field parameters

[17] Van Vleck J H 1968 *J. Phys. A: Math. Gen.* **39** 365

[18] Nieuwpoort W C and Blasse G 1966 *Solid State Commun.* **4** 227

[19] Huang J, Loriers J, Porcher P, Teste de Sagey G, Caro P and Levy-Clement C 1984 *J. Chem. Phys.* **80** 6204